Measuring Electron and Hole Transfer in Core/Shell Nanoheterostructures

Chi-Hung Chuang,[†] Tennyson L. Doane,[†] Shun S. Lo,[‡] Gregory D. Scholes,[‡,*] and Clemens Burda[†,*]

[†]Center for Chemical Dynamics and Nanomaterials Research, Department of Chemistry, Case Western Reserve University, 10900 Euclid Avenue, Cleveland, Ohio 44106, United States, and [‡]Department of Chemistry, 80 St. George Street, Institute for Optical Sciences, and Center for Quantum Information and Quantum Control, University of Toronto, Toronto, Ontario, M5S 3H6 Canada

ABSTRACT Using femtosecond transient absorption and time-resolved photoluminescence spectroscopy, we studied the electron *versus* hole dynamics in photoexcited quasi-type-II heterostructured nanocrystals with fixed CdTe core radii and varying CdSe shell coverage. By choosing the pump wavelength in resonance with the core or the shell states, respectively, we were able to measure the excited electron and hole dynamics selectively. Both, the core- and the shell-excited CdTe/CdSe nanocrystals showed the same spectral emission and photoluminescence lifetimes, indicating that ultrafast electron and hole transfer across the core/shell interface resulted in the identical long-lived charge transfer state. Both charge carriers have subpicosecond transfer rates through the interface, but the subsequent relaxation rates of the hole ($\tau_{dec} \sim 800$ ps) and electron ($\tau_{avg} \sim 8$ ps) are extremely different. On the basis of the presented transient absorption measurements and fitting of the steady-state spectra, we find that the electron transfer occurs in the Marcus inverted region and mixing between the CdTe exciton and charge transfer states takes place and therefore needs to be considered in the analysis.

KEYWORDS: type-II heterostructure · core/shell quantum dots · charge transfer · electron/hole relaxation · femtosecond transient absorption · Marcus theory

Ideal type-II semiconductor heterostructures comprise two components with a staggered band offset. Spatial separation of the electron and hole wave functions within such type-II semiconductor heterostructures[1,2] can result in a long-lived charge transfer (CT) state that has desirable characteristics for applications such as light emitters, lasers, photocatalysts, and photovoltaic devices.[3−8] The long-lived charge separation state can be either obtained by direct excitation of the CT state or by photoexcitation of an exciton followed by charge carrier transfer across the interface. Investigating formation and relaxation of the CT state provides information about the pathways and efficiencies involved. In this context, we have used femtosecond transient absorption (TA) spectroscopy to elucidate ultrafast charge carrier relaxation in each component of heterostructured nanocrystals (NCs) made of a 3.4 nm CdTe core and a CdSe shell that has variable thickness.

A number of studies of electron transfer (ET) across the interface in type-II heterostructures and relaxation to surface defect states have been published over the past few years.[9−23] In a previous study,[13] we demonstrated that ET across the interface of CdTe/CdSe NCs becomes observable and measurable as the CdSe shell approaches the type-II regime, which we experimentally determined to be at 0.4 nm (or one monolayer shell) for a 3.4 nm CdTe core. The dynamics for core, shell, and CT states after excitation in resonance with the core state were analyzed using fits to exponential decay functions. Similarly, electron and hole relaxation in molecule−quantum dot (QD) systems has also attracted a great deal of interest because a molecule−QD conjugate serves as a model system to study charge injection and recombination in light-harvesting systems.[24,25] ET from QDs to conjugated molecules, as well as hole transfer, has been recently observed in molecule−QD conjugates.[26−29]

So far, most studies of carrier dynamics in core/shell systems have focused on the excited state population of electrons.[9−23,30,31] However, relaxation of the hole also plays a significant role in the overall charge redistribution after photoexcitation. Here, we compare for the first time electron *versus* hole kinetics in CdTe/CdSe NCs by selectively pumping the different electronic transitions, as shown in Figure 1. Since the formed excitons are quite sensitive to nanometer confinement—it produces large shifts in the absorption spectra—the electronic absorption of type-II NCs tends to be broad and becomes unresolved because of the combination of the size dispersions of the two materials in the ensemble.

This study specifically targets a series of thin-shell spherical CdTe/CdSe NCs (CdTe/CdSe 1−7; the numbering refers to the increasing shell coverage) that transitions from a type-I to a quasi-type-II regime and continues into the onset of the type-II regime, as

* Address correspondence to burda@case.edu, gscholes@chem.utoronto.ca.

Received for review May 16, 2011 and accepted June 14, 2011.

Published online June 14, 2011
10.1021/nn201788f

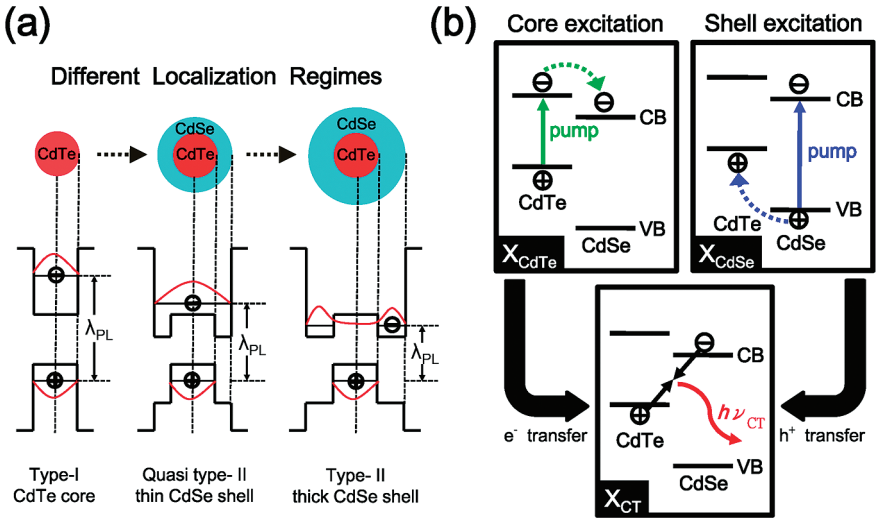

Figure 1. (a) Different localization regimes as a function of shell coverage. The bare CdTe corresponds to the type-I regime, while the thin-shell coverage with an electron delocalized over the entire NC belongs to the quasi-type-II regime. The onset of the type-II regime starts as the electron and hole are separated in the shell and core, respectively. (b) Scheme showing three band-edge states, CdTe, CdSe, and charge transfer state, represented by X_{CdTe}, X_{CdSe}, and X_{CT}, respectively. Black bent arrows indicate transitions between states. Other symbols include valence band (VB), conduction band (CB), electron transfer (green dashed arrow), hole transfer (blue dashed arrow), and charge transfer emission (red arrow).

shown Figure 1a.[17] In the case of bare CdTe core NCs, electron and hole wave functions have centered spatial distributions, typical for the type-I regime. Upon deposition of CdSe on the core, the core/shell system transitions to a quasi-type-II regime (CdTe/CdSe 1−5 NCs) where an electron is delocalized in core and shell. Finally, for the thicker shell systems, CdTe/CdSe 6 and 7 NCs, we find spectroscopically the ET across the interface and electron localization in the shell that is indicative of the onset of the type-II regime. The prepared NCs provide an ideal experimental system for identifying the relative positions of CdTe and CdSe states, which we use to study both the electron and hole dynamics in these core/shell nanoheterostructures. By tuning the excitation resonant with either the CdTe or CdSe band-edge states, we found that one can create excitons selectively in the core or shell (Figure 1b), respectively. The ET from X_{CdTe} leads to the formation of X_{CT}. On the other band, the X_{CT} state can also be obtained by a hole transfer from X_{CdSe}. Therefore, the two initial photoexcited states, X_{CdTe} and X_{CdSe}, which result from core or shell excitation, respectively, relax eventually into the same X_{CT} state (lowest excited state), which was sufficiently emissive to be studied in this work.

In this work, we describe the evolution of the optical properties of CdTe/CdSe core/shell NCs from steady-state UV−vis and photoluminescence (PL) spectroscopy. PL lifetimes of the resulting CT state were measured after selectively pumping the core, shell, and high energy states. On the basis of the framework of Marcus theory, we demonstrate the first analysis of a spherical core/shell system in the quasi-type-II regime. With femtosecond TA measurements, we distinguish between electron and hole relaxation. We conclude that both electrons and holes have subpicosecond transfer rates through the interface, followed by very different relaxation rates.

RESULTS AND DISCUSSION

Steady-state UV−vis and PL spectroscopies were used to explore the electronic state evolution for a series of CdTe/CdSe core/shell NCs with a common CdTe core and increasing CdSe shell coverage. Figure 2a shows the absorption (solid lines) and PL (dashed lines) spectra of CdTe cores and 7 CdTe/CdSe core/shell NCs with increasing shell coverage. As the core is subsequently coated with a CdSe shell, the CdTe exciton band (X_{CdTe}), marked with asterisks, red shifts from 547 to 684 nm and the corresponding PL shifts from 566 to 710 nm. While the red shift may initially appear large, it has been shown by first-principles calculations that the band gap of a core/shell NC with fixed core size narrows upon increased shell coverage due to decreasing confinement and additional strain.[32] In addition, previous experimental work found evidence for strain across the CdSe/CdS interface.[33] The CdSe exciton states (X_{CdSe}) are observed on the blue side of the CdTe absorption (denoted with diamonds). The exciton transitions (X_{CdTe} and X_{CdSe}) and PL wavelengths (λ_{PL}) of the eight prepared NC samples are tabulated in Table 1. In the TA measurements presented below, the core- and shell-excited spectra were obtained using the excitation wavelength at X_{CdTe} and X_{CdSe}, respectively, as listed in Table 1.

We studied the PL lifetime occurring on the nanosecond time scale with a streak camera. Figure 2b shows the PL intensity decay of CdTe/CdSe 5 NCs at 658 nm upon excitation at different wavelengths. We chose three wavelengths, 606, 573, and 470 nm, to excite the CdTe/core, CdSe/shell, and high energy states, respectively, and

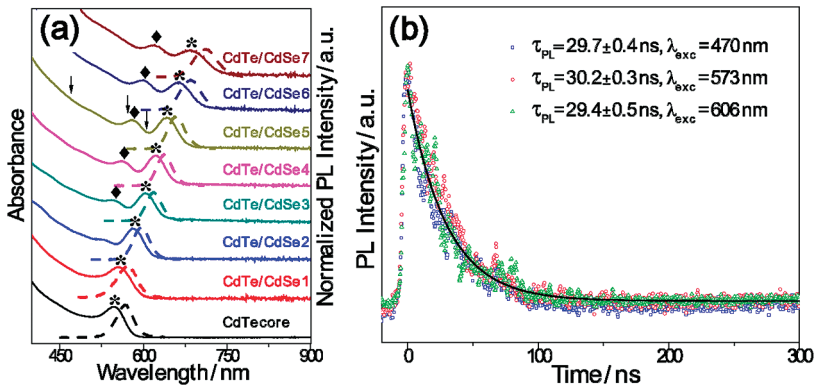

Figure 2. (a) UV−vis absorption (solid lines) and PL (dashed lines) spectra of CdTe/CdSe core/shell heterostructured NCs with a CdTe core and increasing CdSe shell coverage. The numbering of the series refers to increasing shell coverage with increments of ~0.06 nm starting from a 3.4 nm CdTe core to a 4.2 nm CdTe/CdSe 7 NC. The volume percentages of core and shell in CdTe/CdSe 7 NCs are 53 and 47%, respectively. The CdTe core and CdSe shell transitions in the absorption spectra are marked with asterisks (X_{CdTe}) and diamonds (X_{CdSe}), respectively. Absorption and PL spectra are shifted vertically for clarity. (b) PL intensity decay curves of CdTe/CdSe 5 NCs excited by different wavelengths, 470 (blue), 573 (red), and 606 (green) nm. The solid line shows a numerical fit of the PL decay monitored at 658 nm using a single exponential function. The positions of three excitation wavelength for CdTe/CdSe 5 NCs are denoted by arrows in panel (a).

TABLE 1. Summary of the Exciton Transitions and PL Wavelengths of CdTe/CdSe Core/Shell Heterostructured NCs[a]

sample	X_{CdTe}	X_{CdSe}	λ_{PL}	τ_{PL}[b]
CdTe core	547		566	
CdTe/CdSe 1	555		571	
CdTe/CdSe 2	582		595	
CdTe/CdSe 3	603	544	617	
CdTe/CdSe 4	623	560	636	
CdTe/CdSe 5	642	578	658	30
CdTe/CdSe 6	662	599	684	32
CdTe/CdSe 7	684	620	710	35

[a] All spectral wavelengths in nanometers. [b] PL lifetimes in nanoseconds.

monitored the PL lifetimes at a constant wavelength of 658 nm. Excitations at 606 and 573 nm create excitons in CdTe (X_{CdTe}) and CdSe (X_{CdSe}) with configurations depicted in Figure 1b. The PL lifetimes, fit with a single exponential decay function, are 29.4 ± 0.5, 30.2 ± 0.3, and 29.7 ± 0.4 ns corresponding to core, shell, and high energy excitations. This example shows that, independent of the excitation wavelength, the excited CdTe/CdSe NCs relax to a CT state (Figure 1b) and emit at λ_{PL} with a PL lifetime of τ_{PL} (Table 1). The results indicate that charge carrier relaxation involves transitions between X_{CdTe}/X_{CdSe} and X_{CT} states, as depicted in Figure 1b.[34] We obtained PL lifetimes of the CdTe/CdSe 5, 6, and 7 core/shell NCs (Figure S1 and Table S1 in the Supporting Information). They were 30, 32, and 35 ns, respectively. The increase of PL lifetime with shell thickness is consistent with our previous results,[13] where we reported better charge separation upon increasing shell coverage.

To map out the energetics of exciton and CT states, we performed a steady-state spectral analysis based on the framework of Marcus theory.[35,36] Figure 3 shows a deconvolution of the absorption and emission spectra for CdTe/CdSe 7 NCs as an example. Mixed states CT_A and CT_B with either dominant CdTe character and minor CT contribution (CT_A) or *vice versa* (CT_B) were found for both absorption and emission and are consistent with the fact that we measure the NCs in the quasi-type-II regime with a thin one-monolayer CdSe coverage. In other words, the CT and CdTe exciton states are strongly mixed for these core/shell nanoheterostructures. Free energy curves for CdTe/CdSe 7 NCs were obtained by fitting these spectra, as described in detail earlier.[36,37] Following the previous work by one of the authors,[37] we found that the free energy difference is $\Delta G^0_{ET} \sim 32$ meV and the reorganization energy is $\lambda_{CT} \sim 19$ meV (detailed analysis is available in Table S2). The two free energy curves are very close and approximately degenerate. Therefore, we anticipate a strong mixing between CdTe and CT states. The two bands (CT_A and CT_B) we observe in Figure 3a have mixed CdTe and CT character. The CT_A band is dominated by the CdTe character, while the CT_B band has mostly CT state behavior. The resulting adiabatic free energy curves of CT_A and CT_B states are shown in the inset of Figure 3c.

It is interesting to note that the description of state mixing is in accord with the quasi-type-II model, in which one of the charge carriers is delocalized over the entire NC volume.[17] Following this model, core excitation would create excitons in the mixed CdTe−CT states (simultaneously photoexciting the CdTe and CT states) evidenced by the electron dynamics elucidated by the TA measurements presented below. Despite the small free energy difference of 32 meV between the CdTe and CT states in the prepared quasi-type-II CdTe/CdSe NCs, the very small reorganization energy (~19 meV) means that the photoinduced ET reaction occurs in the Marcus inverted region. This analysis shows that ET in both quasi-type-II and type-II

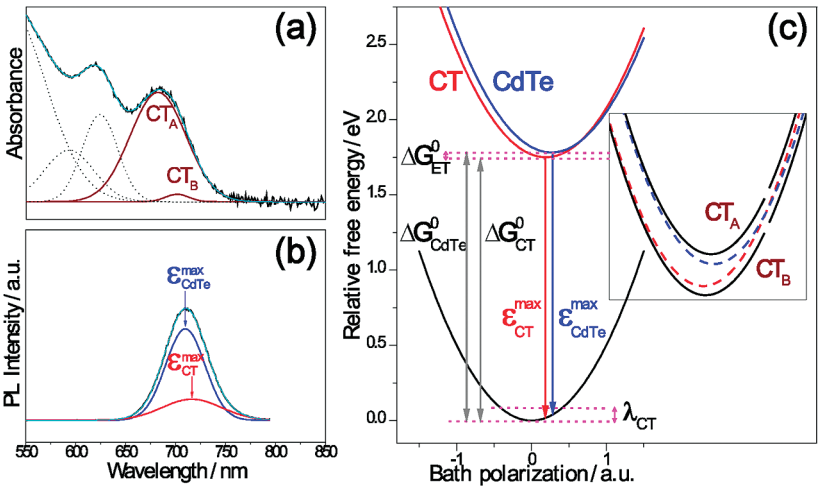

Figure 3. Analysis of the (a) absorption and (b) emission spectra of CdTe/CdSe 7 NCs. The black lines show the experimental line shapes, while the blue, red, and wine colored lines are the fitted curves. The CT_A and CT_B states were obtained along with three bands (dotted lines) for the absorption spectrum; ε^{max}_{CdTe} and ε^{max}_{CT} obtained by deconvolution correspond to the CdTe and CT emission, respectively. (c) Diabatic free energy curves are plotted *versus* bath polarization from analysis of CdTe/CdSe 7 NCs. Various quantities are shown, ΔG^0_{CdTe} and ΔG^0_{CT} are the free energy differences between ground state and the CdTe/CT state, ε^{max}_{CdTe} and ε^{max}_{CT} are the corresponding emission energies, ΔG^0_{ET} and λ_{CT} are the driving force and reorganization energy, respectively, for the ET reaction. The inset shows the adiabatic free energy curves that result from the state mixing.

regimes belongs to reactions in the Marcus inverted region due to inherently small reorganization energies in semiconductor NCs.

Femtosecond TA spectroscopy was used to study the charge carrier transfer in these CdTe/CdSe NCs. Figure 4 shows the TA spectra and kinetics in 3000 and 200 ps time windows as monitored at the core state, as well as the numerical fitting results of CdTe/CdSe 5 NCs. Panels a and b of Figure 4 are the TA spectra measured with core (642 nm) and shell (585 nm) excitation, respectively. The transient spectra recorded for both core and shell excitation conditions are similar, but the kinetics of the bleach decay are distinctly different. We first compare the bleach decay of the core population in a 3000 ps time window. For the core excitation (Figure 4c), the bleach signal amplitude remains almost constant between 200 and 3000 ps. However, in the shell excitation case (Figure 4d), the bleach clearly decays during this time window with a 980 ps time constant. The comparison for different CdTe/CdSe NCs is shown in Figure S3 of the Supporting Information.

The kinetics in a shorter time window of 200 ps (Figure 4e,f) reveal that in each case different charge carriers and pathways are involved in the relaxation of the CdTe core. We find that this decay can be satisfactorily fitted with a biexponential function (red curve in Figure 4e). A similar result was found for the other CdTe/CdSe NCs which is tabulated in Table 2. The TA spectra and kinetics of all CdTe/CdSe NCs are available in the Supporting Information. In contrast, the shell-excited bleaching signals (Figure 4f) keep slowly decaying until 3000 ps, which is the limit of our TA measurement. This extremely slow decay could be fit with a single exponential function with a time constant of ~980 ps (red curve in Figure 4d). The slow decays were also observed in CdTe/CdSe 4, 6, and 7 NCs. An average decay rate of ~800 ps in shell-excited measurements was obtained. We show fitting results for data collected over both 200 and 3000 ps time windows in Figure S4. All kinetics parameters are summarized in Table 2.

In the shell-excited PL lifetime measurement (Figure 2b), the excitation energy (573 nm) is enough to reach the energy states above the CdTe band edge (606 nm), yielding the formation of hot electrons in the core. Given the comparable core and shell volume percentages in CdTe/CdSe 7 NCs (as shown in Figure 2 caption), the probability of exciting shell *versus* core is pretty similar in terms of the total volume of material and comparable oscillator strengths for electronic transitions. Thus, it is observed that the shell establishes an electronic band structure, similar to the band structure that was observed in earlier investigated CdS/HgS/CdS quantum well quantum dots with one monolayer HgS.[38−41]

On the basis of the utilized laser excitation power, each photoexcited NC contains at most one single exciton. While in theory NCs could get excited in the core or shell by shell excitation (*i.e.*, the ensemble would show both core and shell relaxation), we find experimentally that two cases can be distinguished by spectrally choosing excitation wavelengths for either core or shell. We assign the two different relaxation dynamics to electron or hole relaxation, according to the spectral assignments and band-edge alignment. In TA measurements, we monitored the same bleaching at the core wavelength after different wavelength

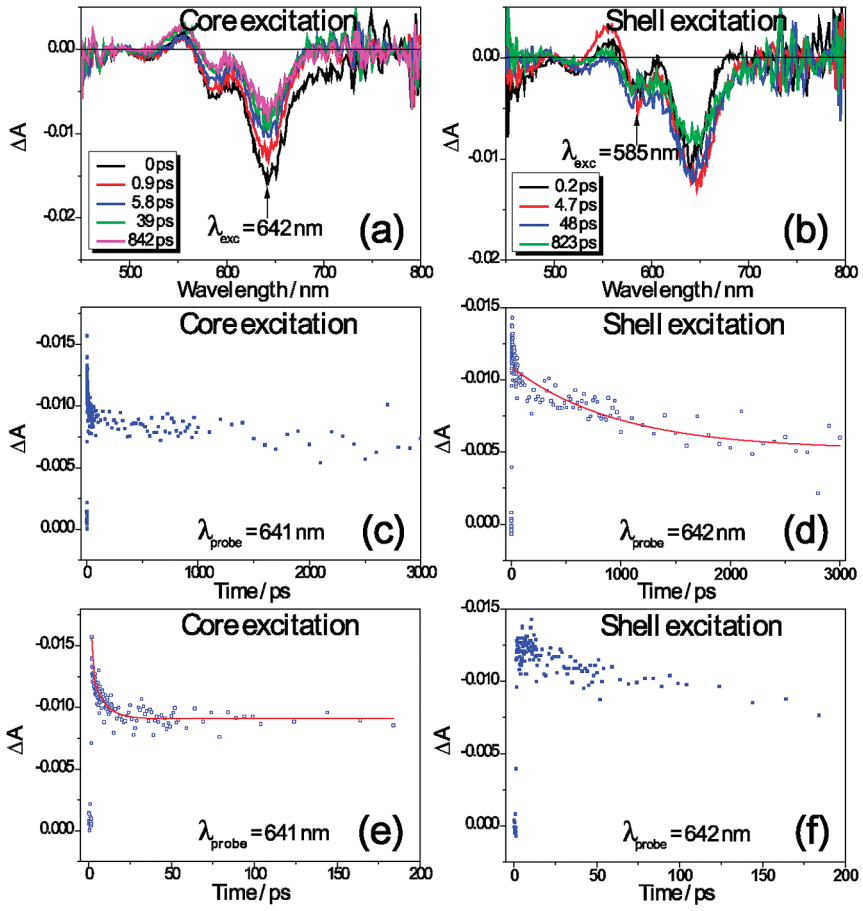

Figure 4. Transient absorption spectra and kinetics monitored at the CdTe (core) state for CdTe/CdSe 5 by core (left) and shell excitation (right). Transient absorption spectra recorded at different delay time after (a) core and (b) shell excitation. The pump−probe delay times of the recorded spectra are shown in the corresponding legends. The arrows indicate pump wavelength, 642 and 585 nm for core and shell excitation, respectively. (c,d) Kinetics at the CdTe (core) state in a 3000 ps time window after excitation at core and shell states, respectively. (e,f) Kinetics at the CdTe (core) state in a 200 ps time window. Red curves in (d) and (e) show numerical fits.

TABLE 2. Analysis of the Kinetic Parameters from Transient Absorption Spectroscopy[a]

	core excitation			shell excitation	
sample	$\tau_{dec,1}$ [b]	$\tau_{dec,2}$ [b]	τ_{avg} [c]	τ_{rise} [d]	τ_{dec} [b]
CdTe core	0.59 ± 0.04 (87%)	9.02 ± 0.85 (13%)	1.7		
CdTe/CdSe 2	<0.3				
CdTe/CdSe 3	0.61 ± 0.07 (68%)	11.4 ± 1.1 (32%)	4.1		
CdTe/CdSe 4	1.55 ± 0.19 (58%)	17.0 ± 1.8 (42%)	8.0	∼1.1	754 ± 260
CdTe/CdSe 5	0.17 ± 0.06 (64%)	7.36 ± 0.87 (36%)	2.8	∼0.5	976 ± 156
CdTe/CdSe 6	1.35 ± 0.35 (53%)	29.1 ± 5.7 (47%)	14.4	∼0.4	790 ± 127
CdTe/CdSe 7	0.40 ± 0.13 (51%)	24.9 ± 4.4 (49%)	12.4	∼0.2	563 ± 101

[a] All the constants are expressed in picoseconds. [b] Measured at $\lambda_{X,CdTe}$ (see Figure 2a and Table 1). [c] The average decay rates, τ_{avg}, are calculated using relative amplitude of $\tau_{dec,1}$ and $\tau_{dec,2}$ shown in parentheses. [d] The τ_{rise} at $\lambda_{X,CT}$ (see Figure 5, 4th column) corresponds to initial bleach kinetics in the core after shell excitation, which we assigned to hole transfer; τ_{rise} is also present after core excitation due to electron transfer, but in each case, rates are at instrument resolution (∼150 fs).

excitation, resonant with the core or shell states, and obtained the kinetic parameters for the core relaxation (Table 2). On the basis of the different decay rates, we rule out the creation of an exciton in the core upon shell excitation; otherwise, we would observe the same time constants for shell excitation ($\tau_{dec,1}$ and $\tau_{dec,2}$ in Table 2) as we found for core excitation. Instead, we obtained a much slower decay rate (τ_{dec} ∼ 800 ps in Table 2) by shell excitation. This indicates that the exciton was indeed created in the CdSe state (X_{CdSe}) *via* shell excitation. On the other hand, core excitation simultaneously photoexcited

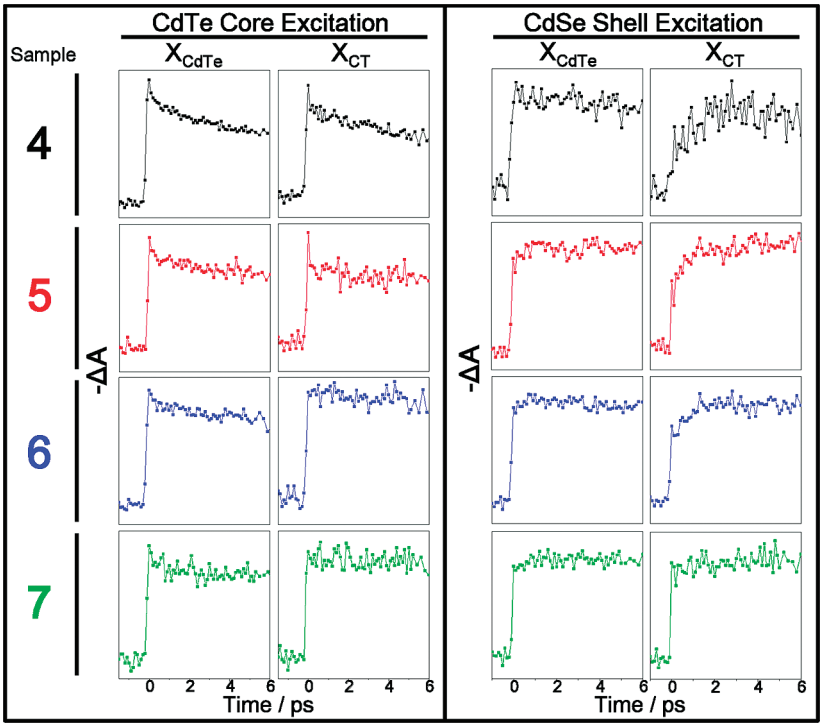

Figure 5. Kinetics measured at $\lambda_{X,CdTe}$ and $\lambda_{X,CT}$ after core (left) and shell (right) excitation and shown in a 6 ps time window for CdTe/CdSe 4−7 NCs. Numbers 4−7 refer to the corresponding core/shell systems from Table 1 and Figure 2. The kinetics of the CT states were monitored 20−25 nm red-shifted from the corresponding CdTe transition; see Figure 3a.[13]

the CdTe and CT states due to state mixing, which we could confirm through the analysis summarized in Figure 3.

In the prevailing theories for the TA signals of QDs, the TA changes (mainly bleaching) at specific wavelengths are a measure for the occupation of the corresponding photoexcited states.[42] In semiconductor QDs, the hole levels are more closely spaced than the electron levels due to the larger valence band effective masses.[43] At sufficiently high temperature, photoexcited holes will be thermally distributed over a large number of levels, resulting in smaller hole occupation numbers per energy level. Therefore, the occupation factor of the bleaching intensity is dominated by the higher occupation of electron states.[44] On the basis of these arguments, we will discuss the electron and hole dynamics observed in our TA measurements separately.

Electron Dynamics. In the case of core-excited TA measurements, the bleach signals at the core state are dominated by electrons in the conduction band for reasons laid out above. We attribute the fast bleach decays ($\tau_{dec,1}$ and $\tau_{dec,2}$ in Table 2) to electron relaxation from the core conduction band to surface and interface-related defect states. The results are consistent with previously reported work.[13,42] In Figure 5, we summarize the kinetic traces of CdTe/CdSe 4 (black), 5 (red), 6 (blue), and 7 (green) NCs on a 6 ps time scale. The kinetics of CdTe/CdSe 1, 2, and 3 NCs are not shown since the shell coverage is too thin to obtain the shell-excited signals. Both columns on the left were obtained by core excitation. In the first column, core-excited kinetics at the X_{CdTe} state, a decreasing amplitude of the fast component ($\tau_{dec,1}$) from CdTe/CdSe 4 to 7 shows the surface passivation effect by growing the CdSe shell. Surface passivation blocks the electron relaxation into metal dangling-bond-related defects. In CdTe/CdSe 4 and 5 NCs, we observed decays at the CdTe and CT states since we simultaneously populated states where the CdTe and CT states are mixed. This is the first direct experimental evidence of the state mixing (predicted by our energetic analysis) in a semiconductor core/shell nanoheterostructure. With the same excitation wavelength, we observed with increasing shell coverage (second column in Figure 5) a fast decay dynamics followed by the population of the CT state. The onset of type-II behavior in CdTe/CdSe 6 and 7 NCs initiated ET across the interface, resulting in the buildup of transient signals at the CT transition wavelength.[13] Population of the CT state has a rise time on the subpicosecond time scale, which is indicative of the expected ET across the CdTe/CdSe interface. Both columns of the core-excited kinetics in Figure 5 reveal the electron dynamics of CdTe/CdSe NCs.

Hole Dynamics. Selective excitation of the shell states did not directly generate carriers in the core (Figure 1b). However, we still observed formation of bleach signals from the core. All samples exhibited subpicosecond population buildup, with faster rise times (τ_{rise}) with increasing shell coverage (Table 2). In CdTe/CdSe

quasi-type-II systems, it is unlikely that electrons transfer from the shell to the core because CdSe has an inherently lower conduction band energy. In contrast, the hole has sufficient driving force (valence band offset between CdTe and CdSe) to undergo charge transfer and form a CT configuration. Therefore, selective photoexcitation of the CdSe shell states leads to a bleaching signal that can be monitored at core CdTe states, and the rise kinetics in the first 6 ps must be due to hole transfer from the shell across the interface to the core. The hole population in the valence band of the core (Figure 1b) results in the observed bleach signals in the TA spectra. The rise of the CT state populations can be clearly seen in the fourth column of Figure 5. The faster rise times with increasing shell coverage indicate the onset of type-II behavior. After the hole transfer, the slow decay kinetics at the core, for which we observed an average decay constant of ~800 ps (Figure 4d), are proposed to be the hole relaxation from the core's valence band to interfacial or intrinsic trapped states. Compared with electron dynamics, we found the hole has a much slower relaxation rate than the electron does. This is important for photocatalytic and photovoltaic systems where electron and hole relaxation matter because both photoexcited carriers contribute to the overall charge distribution.

The explanation follows classical thermodynamic theory (Gibbs' free energy) and is consistent with our PL lifetime studies. On the basis of the TA results, we found that the hole transfer rate is slightly slower than the ET rate, although both are on the subpicosecond time scale. Interestingly, in contrast to the electron relaxation (τ_{avg}) to surface states, the hole relaxation time constant is much longer (τ_{dec}). This difference in behavior between electron and hole relaxation has been observed earlier.[45] Here, by selectively choosing the pump wavelength resonant with the core or the shell states, we are able to obtain the electron and hole dynamics separately using both TA and PL measurements.

CONCLUSIONS

In this study of CdTe/CdSe quasi-type-II heterostructures, we investigated electron and hole dynamics by selectively choosing pump wavelengths in resonance with core and shell states, respectively. The PL lifetime measurements have shown that both core- and shell-excited NCs lead to long-lived CT states by electron and hole transfer across the interface, respectively. With TA spectroscopy, we find that the electron and hole dynamics can be distinguished, both of which have subpicosecond transfer rates yielding a CT state for which we observed the buildup dynamics on the subpicosecond time scale. The electron undergoes fast relaxation (~8 ps) to surface defect states in case of core excitation, while the shell-excited hole undergoes a slow decay process (~800 ps) after transferring to the core state. The difference may be related to the more localized nature of the hole wave function. This study provides a detailed analysis of photoinduced ET reactions occurring in the Marcus inverted region for spherical core/shell quantum dots. Electron and hole kinetics were identified, and mixing between the CdTe and CT states was experimentally demonstrated.

EXPERIMENTAL SECTION

Chemicals. Cadmium oxide (99%, Strem Chemicals), selenium (99.5%, Aldrich), tellurium (99.997%, Aldrich), 1-octadecene (ODE, 90%, Aldrich), trioctylphosphine (TOP, 90%, Aldrich), 1-tetradecylphosphonic acid (TDPA, 98%, Alfa Aesar), toluene (99.9%, Fischer Scientific), and 2-propanol (99.9%, Fischer Scientific) were used as purchased.

Synthesis of CdTe and CdTe/CdSe Nanocrystals. We followed a procedure described in ref 13 to synthesize CdTe and CdTe/CdSe NCs. A 48 mg amount of CdO was dissolved in a mixture of 1-tetradecylphosphonic acid (TDPA, ~180 mg) and 1-octadecene (ODE, ~22 mL) by first evacuating at 80 °C for 1 h. Then, the mixture was refluxed at 285 °C under an Ar atmosphere until the mixture became optically clear. The Te−TOP solution (50 mg in 2.5 mL of TOP) was rapidly injected at 200 °C. The NCs were allowed to grow at 200 °C for 4 min, and the reaction was terminated by removing the heating mantle. As the solution cooled to room temperature, the CdTe NCs were washed by adding 2-propanol to precipitate. The CdTe NCs were redispersed in toluene for shell coating.

For the core/shell synthesis, we prepared solutions A, B, and C in advance. Solution A was prepared by adding 38 mg of CdO and 141 mg of TDPA in 15 mL of ODE. Solution B was prepared by adding 42 mg of Se in 2.5 mL of TOP. The CdTe NCs (~8 mL) obtained above and 38 mg of the TDPA mixture were added to 27 mL of ODE to form solution C. Solution A was first degassed at 80 °C for 1 h followed by refluxing at 285 °C under Ar atmosphere for 40 min. Solution A was cooled to room temperature under Ar atmosphere. At the same time, solution C was degassed at 80 °C for 90 min, followed by adding 1.4 mL of mixture A + B. Then, solution C was heated to 230 °C for CdSe shell coating. The injection rate of the A + B mixture was kept at ~0.15 mL/min to allow the CdSe shell to nucleate gradually on the seed QDs. After every ~1.3 mL injection, an aliquot was taken out. We obtained a series of CdTe/CdSe heterostructure NCs with CdTe as the core and varying CdSe shell coverage labeled as CdTe/CdSe 1−7. All of the CdTe/CdSe NCs were washed by adding 2-propanol to precipitate and redispersed in toluene for further measurements. The core/shell synthesis did not result in nucleation of separate CdSe NCs. Details are shown in the Supporting Information.

Characterization. UV−vis absorption and PL spectra were recorded using a Varian Cary 50 and Varian Eclipse fluorescence spectrometer, respectively. Typical morphological characterization of CdTe/CdSe NCs by transmission electron microscopy has been shown in our previous work.[13] Femtosecond TA measurements were conducted using a Clark MXR 2001 fs laser system producing 780 nm, 150 fs pulses from a regenerative amplifier. The laser pulse train was split to generate a white light continuum probe pulse in a sapphire crystal and a tunable pump pulse. For TA and PL lifetime experiments, the tunable pump pulse was generated using an optical parametric amplifier (TOPAS, Lightconversion). PL dynamics were measured with a time-resolved streak camera (Optronis) equipped with a monochromator (DK240 0.25 m, Spectral Products). All femtosecond laser experiments were carried out in a 2 mm quartz cuvette at room temperature. The instrumental time resolution

was determined to ~150 fs *via* a pump–probe cross-correlation analysis. The excitation power in both TA (~150 $\mu J/cm^2$ per pulse fluence) and PL lifetime (~50 $\mu J/cm^2$ per pulse fluence) measurements was considered carefully to ensure that the average number of excitations is less than one.

Acknowledgment. C.B. gratefully acknowledges partial support of this research through NSF Career (CHE-0239688) and NIRT (CTS-0608896) grants.

Supporting Information Available: PL intensity decay curves fit with single exponential functions; summary of the PL lifetimes for CdTe/CdSe 5, 6, and 7 NCs; summary of analysis of energetics for CdTe/CdSe 7 NCs; TA spectra of CdTe and CdTe/CdSe NCs; comparison of kinetics in 3000 and 200 ps time windows; bleach decay fit with single exponential and biexponential decay functions. This material is available free of charge *via* the Internet at http://pubs.acs.org.

REFERENCES AND NOTES

1. Lo, S. S.; Mirkovic, T.; Chuang, C.-H.; Burda, C.; Scholes, G. D. Emergent Properties Resulting from Type-II Band Alignment in Semiconductor Nanoheterostructures. *Adv. Mater.* **2011**, *23*, 180–197.
2. Kim, S.; Fisher, B.; Eisler, H.-J.; Bawendi, M. Type-II Quantum Dots: CdTe/CdSe(Core/Shell) and CdSe/ZnTe(Core/Shell) Heterostructures. *J. Am. Chem. Soc.* **2003**, *125*, 11466–11467.
3. Klimov, V. I.; Ivanov, S. A.; Nanda, J.; Achermann, M.; Bezel, I.; McGuire, J. A.; Piryatinski, A. Single-Exciton Optical Gain in Semiconductor Nanocrystals. *Nature* **2007**, *447*, 441–446.
4. Huynh, W. U.; Dittmer, J. J.; Alivisatos, A. P. Hybrid Nanorod–Polymer Solar Cells. *Science* **2002**, *295*, 2425–2427.
5. Acharya, K. P.; Alabi, T. R.; Schmall, N.; Hewa-Kasakarage, N. N.; Kirsanova, M.; Nemchinov, A.; Khon, E.; Zamkov, M. Linker-Free Modification of TiO_2 Nanorods with PbSe Nanocrystals. *J. Phys. Chem. C* **2009**, *113*, 19531–19535.
6. Hyun, B.-R.; Zhong, Y.-W.; Bartnik, A. C.; Sun, L.; Abruna, H. D.; Wise, F. W.; Goodreau, J. D.; Matthews, J. R.; Leslie, T. M.; Borrelli, N. F. Electron Injection from Colloidal PbS Quantum Dots into Titanium Dioxide Nanoparticles. *ACS Nano* **2008**, *2*, 2206–2212.
7. Acharya, K. P.; Hewa-Kasakarage, N. N.; Alabi, T. R.; Nemitz, I.; Khon, E.; Ullrich, B.; Anzenbacher, P.; Zamkov, M. Synthesis of PbS/TiO_2 Colloidal Heterostructures for Photovoltaic Applications. *J. Phys. Chem. C* **2010**, *114*, 12496–12504.
8. Kumar, S.; Jones, M.; Lo, S. S.; Scholes, G. D. Nanorod Heterostructures Showing Photoinduced Charge Separation. *Small* **2007**, *3*, 1633–1639.
9. Dooley, C. J.; Dimitrov, S. D.; Fiebig, T. Ultrafast Electron Transfer Dynamics in CdSe/CdTe Donor–Acceptor Nanorods. *J. Phys. Chem. C* **2008**, *112*, 12074–12076.
10. Hewa-Kasakarage, N. N.; Kirsanova, M.; Nemchinov, A.; Schmall, N.; El-Khoury, P. Z.; Tarnovsky, A. N.; Zamkov, M. Radiative Recombination of Spatially Extended Excitons in (ZnSe/CdS)/CdS Heterostructured Nanorods. *J. Am. Chem. Soc.* **2009**, *131*, 1328–1334.
11. Rawalekar, S.; Kaniyankandy, S.; Verma, S.; Ghosh, H. N. Ultrafast Charge Carrier Relaxation and Charge Transfer Dynamics of CdTe/CdS Core–Shell Quantum Dots As Studied by Femtosecond Transient Absorption Spectroscopy. *J. Phys. Chem. C* **2010**, *114*, 1460–1466.
12. Hewa-Kasakarage, N. N.; El-Khoury, P. Z.; Tarnovsky, A. N.; Kirsanova, M.; Nemitz, I.; Nemchinov, A.; Zamkov, M. Ultrafast Carrier Dynamics in Type II ZnSe/CdS/ZnSe Nanobarbells. *ACS Nano* **2010**, *4*, 1837–1844.
13. Chuang, C.-H.; Lo, S. S.; Scholes, G. D.; Burda, C. Charge Separation and Recombination in CdTe/CdSe Core/Shell Nanocrystals as a Function of Shell Coverage: Probing the Onset of the Quasi Type-II Regime. *J. Phys. Chem. Lett.* **2010**, *1*, 2530–2535.
14. He, J.; Zhong, H.; Scholes, G. D. Electron–Hole Overlap Dictates the Hole Spin Relaxation Rate in Nanocrystal Heterostructures. *Phys. Rev. Lett.* **2010**, *105*, 046601.
15. Peng, P.; Milliron, D. J.; Hughes, S. M.; Johnson, J. C.; Alivisatos, A. P.; Saykally, R. J. Femtosecond Spectroscopy of Carrier Relaxation Dynamics in Type II CdSe/CdTe Tetrapod Heteronanostructures. *Nano Lett.* **2005**, *5*, 1809–1813.
16. Chou, P.-T.; Chen, C.-Y.; Cheng, C.-T.; Pu, S.-C.; Wu, K.-C.; Cheng, Y.-M.; Lai, C.-W.; Chou, Y.-H.; Chiu, H.-T. Spectroscopy and Femtosecond Dynamics of Type-II CdTe/CdSe Core–Shell Quantum Dots. *Chem. Phys. Chem.* **2006**, *7*, 222–228.
17. Ivanov, S. A.; Piryatinski, A.; Nanda, J.; Tretiak, S.; Zavadil, K. R.; Wallace, W. O.; Werder, D.; Klimov, V. I. Type-II Core/Shell CdS/ZnSe Nanocrystals: Synthesis, Electronic Structures, and Spectroscopic Properties. *J. Am. Chem. Soc.* **2007**, *129*, 11708–11719.
18. Zhong, H.; Zhou, Y.; Yang, Y.; Yang, C.; Li, Y. Synthesis of Type II CdTe–CdSe Nanocrystal Heterostructured Multiple-Branched Rods and Their Photovoltaic Applications. *J. Phys. Chem. C* **2007**, *111*, 6538–6543.
19. Chin, P. T. K.; De Mello Donega, C.; Van Bavel, S. S.; Meskers, S. C. J.; Sommerdijk, N. J. M.; Janssen, R. A. J. Highly Luminescent CdTe/CdSe Colloidal Heteronanocrystals with Temperature-Dependent Emission Color. *J. Am. Chem. Soc.* **2007**, *129*, 14880–14886.
20. He, J.; Lo, S. S.; Kim, J. H.; Scholes, G. D. Control of Exciton Spin Relaxation by Electron–Hole Decoupling in Type-II Nanocrystal Heterostructures. *Nano Lett.* **2008**, *8*, 4007–4013.
21. Goebl, J. A.; Black, R. W.; Puthussery, J.; Giblin, J.; Kosel, T. H.; Kuno, M. Solution-Based II–VI Core/Shell Nanowire Heterostructures. *J. Am. Chem. Soc.* **2008**, *130*, 14822–14833.
22. Bang, J.; Chon, B.; Won, N.; Nam, J.; Joo, T.; Kim, S. Spectral Switching of Type-II Quantum Dots by Charging. *J. Phys. Chem. C* **2009**, *113*, 6320–6323.
23. Osovsky, R.; Cheskis, D.; Kloper, V.; Sashchiuk, A.; Kroner, M.; Lifshitz, E. Continuous-Wave Pumping of Multiexciton Bands in the Photoluminescence Spectrum of a Single CdTe–CdSe Core–Shell Colloidal Quantum Dot. *Phys. Rev. Lett.* **2009**, *102*, 197401.
24. O'Regan, B.; Grätzel, M. A Low-Cost, High-Efficiency Solar Cell Based on Dye-Sensitized Colloidal TiO_2 Films. *Nature* **1991**, *353*, 737–740.
25. Kamat, P. V. Quantum Dot Solar Cells. Semiconductor Nanocrystals as Light Harvesters. *J. Phys. Chem. C* **2008**, *112*, 18737–18753.
26. Huang, J.; Stockwell, D.; Huang, Z.; Mohler, D. L.; Lian, T. Photoinduced Ultrafast Electron Transfer from CdSe Quantum Dots to Re-Bipyridyl Complexes. *J. Am. Chem. Soc.* **2008**, *130*, 5632–5633.
27. Blackburn, J. L.; Selmarten, D. C.; Ellingson, R. J.; Jones, M.; Micic, O.; Nozik, A. J. Electron and Hole Transfer from Indium Phosphide Quantum Dots. *J. Phys. Chem. B* **2005**, *109*, 2625–2631.
28. Huang, J.; Huang, Z.; Jin, S.; Lian, T. Exciton Dissociation in CdSe Quantum Dots by Hole Transfer to Phenothiazine. *J. Phys. Chem. C* **2008**, *112*, 19734–19738.
29. Sykora, M.; Petruska, M. A.; Alstrum-Acevedo, J.; Bezel, I.; Meyer, T. J.; Klimov, V. I. Photoinduced Charge Transfer between CdSe Nanocrystal Quantum Dots and Ru-Polypyridine Complexes. *J. Am. Chem. Soc.* **2006**, *128*, 9984–9985.
30. Lupo, M. G.; Della Sala, F.; Carbone, L.; Zavelani-Rossi, M.; Fiore, A.; Luer, L.; Polli, D.; Cingolani, R.; Manna, L.; Lanzani, G. Ultrafast Electron–Hole Dynamics in Core/Shell CdSe/CdS Dot/Rod Nanocrystals. *Nano Lett.* **2008**, *12*, 4582–4587.
31. Oron, D.; Kazes, M.; Banin, U. Multiexcitons in Type-II Colloidal Semiconductor Quantum Dots. *Phys. Rev. B* **2007**, *75*, 035330.
32. Yang, S.; Prendergast, D.; Neaton, J. B. Strain-Induced Band Gap Modification in Coherent Core/Shell Nanostructures. *Nano Lett.* **2010**, *10*, 3156–3162.
33. Chen, X.; Lou, Y.; Samia, A. C.; Burda, C. Coherency Strain Effects on the Optical Response of Core/Shell Heteronanostructures. *Nano Lett.* **2003**, *3*, 799–803.
34. Jones, M.; Kumar, S.; Lo, S. S.; Scholes, G. D. Exciton Trapping and Recombination in Type II CdSe/CdTe Nanorod Heterostructures. *J. Phys. Chem. C* **2008**, *112*, 5423–5431.

35. Marcus, R. A.; Sutin, N. Electron Transfers in Chemistry and Biology. *Biochim. Biophys. Acta* **1985**, *811*, 265–322.
36. Marcus, R. A. Relation between Charge Transfer Absorption and Fluorescence Spectra and the Inverted Region. *J. Phys. Chem.* **1989**, *93*, 3078–3086.
37. Scholes, G. D.; Jones, M.; Kumar, S. Energetics of Photoinduced Electron-Transfer Reactions Decided by Quantum Confinement. *J. Phys. Chem. C* **2007**, *111*, 13777–13785.
38. Braun, M.; Burda, C.; El-Sayed, M. A. Variation of the Thickness and Number of Wells in the CdS/HgS/CdS Quantum Dot Quantum Well System. *J. Phys. Chem. A* **2001**, *105*, 5548–5551.
39. Braun, M.; Burda, C.; Mohamed, M.; El-Sayed, M. A. Femtosecond Time-Resolved Electron−Hole Dynamics and Radiative Transitions in the Double-Layer Quantum Well of the CdS/$(HgS)_2$/CdS Quantum-Dot-Quantum-Well Nanoparticle. *Phys. Rev. B* **2001**, *64*, 035317.
40. Braun, M.; Link, S.; Burda, C.; El-Sayed, M. A. Determination of the Localization Times of Electrons and Holes in the HgS Well in a CdS/HgS/CdS Quantum Dot−Quantum Well Nanoparticle. *Phys. Rev. B* **2002**, *66*, 205312.
41. Braun, M.; Link, S.; Burda, C.; El-Sayed, M. A. Transfer Times of Electrons and Holes Across the Interface in CdS/HgS/CdS Quantum Dot Quantum Well Nanoparticles. *Chem. Phys. Lett.* **2002**, *361*, 446–452.
42. Klimov, V. I.; McBranch, D. W.; Leatherdale, C. A.; Bawendi, M. G. Electron and Hole Relaxation Pathways in Semiconductor Quantum Dots. *Phys. Rev. B* **1999**, *60*, 13740–13749.
43. Ekimov, A. I.; Hache, F.; Schanne-Klein, M. C.; Ricard, D.; Flytzanis, C.; Kudryavtsev, I. A.; Yazeva, T. V.; Rodina, A. V.; Efros, Al. L. Absorption and Intensity-Dependent Photoluminescence Measurements on CdSe Quantum Dots: Assignment of the First Electronic Transitions. *J. Opt. Soc. Am. B* **1993**, *10*, 100–107.
44. Hunsche, S.; Dekorsy, T.; Klimov, V.; Kurz, H. Ultrafast Dynamics of Carrier-Induced Absorption Changes in Highly-Excited CdSe Nanocrystals. *Appl. Phys. B: Laser Opt.* **1996**, *62*, 3–10.
45. Burda, C.; Link, S.; Mohamed, M.; El-Sayed, M. A. The Relaxation Pathways of CdSe Nanoparticles Monitored with Femtosecond Time-Resolution from the Visible to the IR: Assignment of the Transient Features by Carrier Quenching. *J. Phys. Chem. B* **2001**, *105*, 12286–12292.